

Ultrafast Strain-Induced Charge Transport in Semiconductor Superlattices

F. Wang,^{1,2,*} C.L. Poyser,² M.T. Greenaway¹,¹ A.V. Akimov¹,² R.P. Campion,² A.J. Kent,²
T.M. Fromhold,² and A.G. Balanov¹

¹Department of Physics, Loughborough University, Loughborough LE11 3TU, United Kingdom

²School of Physics and Astronomy, University of Nottingham, Nottingham NG7 2RD, United Kingdom



(Received 27 March 2020; revised 25 August 2020; accepted 31 August 2020; published 20 October 2020)

We investigate the effect of hypersonic ($> 1\text{-GHz}$) acoustic phonon wave packets on electron transport in a semiconductor superlattice. Our quantum-mechanical simulations demonstrate that a gigahertz train of picosecond deformation-strain pulses propagating through a superlattice can generate current oscillations the frequency of which is many times higher than that of the strain pulse train, potentially reaching the terahertz regime. The shape and polarity of the calculated current pulses agree well with experimentally measured electric signals. The calculations also explain and accurately reproduce the measured variation of the induced-current-pulse magnitude with the strain-pulse amplitude and applied bias voltage. Our results open a route to developing acoustically driven semiconductor superlattices as sources of millimeter and submillimeter electromagnetic waves.

DOI: 10.1103/PhysRevApplied.14.044037

I. INTRODUCTION

The development of picosecond techniques for generating ultrafast coherent phonons [1,2] has provided researchers with efficient acoustoelectric tools for controlling charge transport in semiconductor nanostructures (for a review, see Ref. [3]). For example, acoustoelectric effects have been proposed for the generation [4–7], heterodyne mixing [8], and detection [9,10] of high-frequency electromagnetic waves. Acoustoelectric pumps have also been used to control quantum phenomena in nanostructures and quantum dots [11–16], with recent experiments demonstrating that ultrafast acoustic pulses can substantially enhance the emission output of a quantum-dot cavity [17,18]. Also, semiconductor nanostructures can serve as active media for transforming terahertz acoustic waves into submillimeter electromagnetic radiation [19,20]. It has also been recently shown that gigahertz strain pulses can be rectified by a semiconductor superlattice (SL), producing a dc response similar to that due to rectification of microwaves [21]. Despite this progress in understanding the gigahertz-terahertz acoustoelectric phenomena, the induced high-frequency charge transport and the corresponding electronic response to changing the parameters of the strain pulses have not yet been widely considered. In particular, it is still unclear how the coherent acoustic and/or strain stimuli affect the

quantum tunneling of the charge and the resulting current-flow dynamics.

In this paper, we present a quantum-mechanical theory of electron transport in a biased weakly coupled SL driven by a coherent phonon wave packet in the form of a train of ultrafast (picosecond) strain pulses. We solve numerically the Schrödinger equation with a time-dependent potential generated by propagating deformation pulses. Our simulations show that the polarity and the magnitude of the generated current response depend on the amplitude of the strain pulses and on the applied bias voltage. The results of our numerical modeling agree well with the experimental measurements of the electrical signals from the SL that we present. We also discuss how the high-frequency electronic response of the SL to coherent acoustic phonons differs fundamentally from the effects of electromagnetic radiation on the SL. This difference is due to the finite propagation time of the phonons through the SL. Finally, our theoretical analysis predicts that the acoustic stimuli can induce current oscillations in the device, with frequencies many times higher than that of the strain pulse train itself and reaching the gigahertz-terahertz regime. The high-frequency oscillations of the current reflect those of the drifting electrons within the alternating acoustic potential propagating along the SL.

The paper has the following structure. In Sec. II, we present our quantum model and numerical simulations of electron transport in a voltage-biased SL driven by strain pulses. We present the results and related discussion in Sec. III. Section IV provides conclusions and an outlook.

*f.wang@nottingham.ac.uk

II. THEORETICAL MODEL

In our study, we model the experiment described in detail in Ref. [21]. The device is schematically pictured in Fig. 1(a). The SL region of length $L = 490$ nm is formed by 50 GaAs and AlAs layers with thicknesses of 5.9 and 3.9 nm, respectively, giving a lattice period of $d = 9.8$ nm. The bias voltage V_0 is applied to the ohmic contacts. The train of strain pulses is generated by femtosecond laser pulses incident on an Al film with thickness 30 nm, deposited on the reverse of the SL GaAs substrate. We estimate the strain-amplitude value using previous experimental measurements [22], where it has been shown that the maximum strain amplitude $\epsilon_a = 10^{-4}$ corresponds to a laser-pulse energy density of approximately 1 mJ cm^{-2} . The time-dependent current $I(t)$ is measured using a digitizing oscilloscope with a 12.5-GHz bandwidth. All measurements are performed at a lattice temperature of $T = 5$ K.

To calculate charge transport in the SL, we solve numerically the time-dependent Schrödinger equation

$$-i\hbar \frac{\partial \psi(x, t)}{\partial t} = \hat{H}\psi(x, t), \quad (1)$$

for the electron wave function $\psi(x, t)$, taking the Hamiltonian to be

$$\hat{H} = -\frac{\hbar^2}{2m} \frac{\partial^2}{\partial x^2} + U_{\text{SL}}(x) - eV_0x + U_a(x, t),$$

where $m = 0.067m_e$ (m_e is the electron mass) is the electronic effective mass in GaAs, e is the electron charge, V_0 is the bias voltage applied to the SL, $U_{\text{SL}}(x)$ is the SL potential, and $U_a(x, t)$ is the time-dependent potential-energy field generated by the deformation pulses [see the

inset in Fig. 1(b)], which includes reflections of the acoustic wave from the boundaries and is given, together with the corresponding parameters, by Eq. (7) in Ref. [21]. This potential propagates along the SL with the speed of sound in GaAs/AlAs layers $v_s \approx 5000$ m/s. To integrate Eq. (1) we use the Crank-Nicolson method, adapted for general-purpose computing on graphics processing units (GPGPU) using the CUDA platform. From $\psi(x, t)$, we calculate the expectation value of the electron displacement $\langle x \rangle$. With no acoustic wave ($U_a = 0$), a nonzero bias $V_0 \neq 0$ induces Bloch oscillations with a frequency proportional to V_0 and an amplitude inversely proportional to V_0 [23].

To calculate the dc current, I_0 , in the SL with no acoustic stimulus applied, i.e., $U_a = 0$, we introduce the drift velocity v_d of the electrons using the Esaki-Tsu formalism [24], which we have used previously to determine and explain measurable SL transport characteristics from underlying Hamiltonian dynamics, for example, stochastic webs [25–29], in the collision-free limit:

$$v_d = \delta \int_0^\infty \frac{dt}{\tau} \langle v(t) \rangle e^{-t/\tau}. \quad (2)$$

This equation takes into account the effect of electron scattering via the parameters $\tau = \tau_i\delta = 0.47$ ps and $\delta = \sqrt{\tau_e/(\tau_i + \tau_e)} = 12.9$, which depend on the inelastic, τ_i , and elastic, τ_e , scattering times [25]. The electron velocity $\langle v(t) \rangle$ is found by averaging $d \langle x \rangle / dt$ over different initial phases of the Bloch oscillations in the interval $[0, 2\pi]$. The dc electric current in the SL is $I_0 = \pi r^2 n_e v_d$, where $r = 50 \mu\text{m}$ is the radius of the SL mesa and $n_e = 10^{17} \text{ cm}^{-3}$ is the doping density. The effect of the ohmic contacts is taken into account by setting $V_0 = V_{\text{SL}} - I_0 R_c$, where V_{SL}

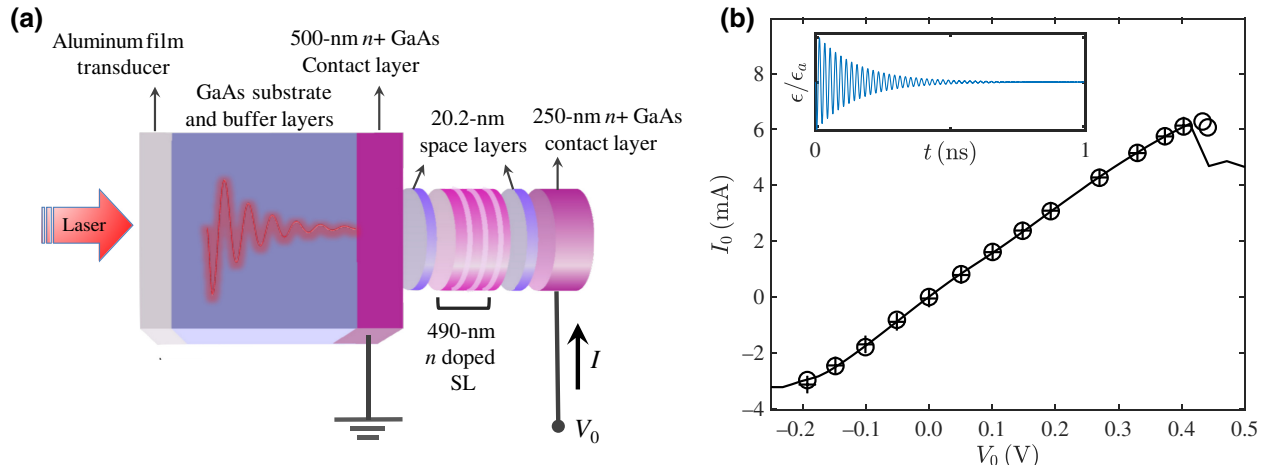


FIG. 1. (a) A schematic diagram of our device, which includes (toward the right) the weakly coupled SL, contacts and spacer layers. The optoelectric Al film transducer (left) is deposited on the side of the GaAs substrate opposite to the device. (b) The current-voltage characteristics, $I_0(V_0)$, of the device calculated numerically (open circles), approximated by a cubic polynomial (crosses) and measured experimentally (solid curve); the inset shows the numerically simulated time realization of strain pulses with a frequency of 46 GHz generated by the Al film transducer, where ϵ_a is the maximum strain within the train of pulses.

is the voltage drop across the SL and $R_c = 54.7\Omega$ is the contact resistance.

The time-dependent current $I(t) = \pi r^2 n_e e v_d(t)$ generated by the voltage-biased SL driven by the strain pulses is calculated using the time-dependent drift velocity [30]

$$v_d(t) = \int_{-\infty}^t \frac{dt_0}{\tau} \langle v(t) \rangle e^{-(t-t_0)/\tau}. \quad (3)$$

To study the response of the SL to strain stimuli, we analyse the incremental current $\delta I(t) = I(t) - I_0$.

III. RESULTS AND DISCUSSION

The solid black curve in Fig. 1(b) shows the current-voltage characteristic, $I_0(V_0)$, measured for the SL used in our experiments and the parameters of which [see Fig. 1(a) and Sec. II] are used in the model given by Eqs. (1)–(3) and the resulting numerical simulations. For V_0 between -0.2 and $+0.4$ V, I_0 grows monotonically with increasing V_0 . However, when $V_0 > 0.4$ V, an electric instability results from the onset of negative differential conductivity (NDC) [31], which induces propagating charge domains and associated current self-oscillations [26,32]. In order to avoid these propagating charge domains affecting and complicating our measurements and analysis, we ensure that $|V_0| \leq 300$ mV. The measured $I_0(V_0)$ characteristic is used to determine τ and δ (see Sec. II) by fitting the corresponding calculated curve to it. As shown in Fig. 1(b), the model given by Eqs. (1)–(2) (empty circles) reproduces the measured $I_0(V_0)$ curve accurately.

Typical $\delta I(t)$ current pulses calculated numerically for $\epsilon_a = 1.5 \times 10^{-4}$ and $V_0 = 100$ mV, 0 mV and -100 mV are shown by the gray solid curves in Figs. 2(a), 2(b) and 2(c), respectively. Our calculations reveal fast oscillations with a frequency that is several (approximately 4) times larger than the 46-GHz frequency of the acoustic oscillations. Notably, our results are qualitatively different from the case of a SL driven by an electromagnetic wave [31,33], which responds only to the fundamental frequency (and harmonics) of the ac driving field. Figure 2(d) shows the Fourier spectra calculated for the signals in Figs. 2(a)–2(c). All three spectra reveal a sharp peak at a frequency (190 GHz) that is far higher than the frequency of the picosecond pulse train (46 GHz). Our quantum simulations show that this originates from slow propagation of the strain pulses, which, in contrast to the case of electromagnetic driving (see the Appendix), cannot be neglected. Figure 2(e) illustrates the dynamics of the wave packet $|\psi(x, t)|^2$ as it travels through the SL. Initially, it is accelerated by the acoustic wave incident on the SL, but after approximately 1.5 ns the wave packet slows due to the decay of the acoustic pulse [see the inset in Fig. 1(b)]. However, for $t \leq 1.5$ ns, the wave packet travels with an almost constant mean speed (approximately 17.8 m/s), while also demonstrating small superimposed high-frequency oscillations: see the averaged electron trajectory $\langle x \rangle(t)$ in Fig. 2(e) and its inset.

Similar behavior has previously been predicted in Ref. [6], where it has also been shown that electron miniband transport induced by a plane acoustic wave can up-convert the frequency of the wave, into faster electron oscillations,

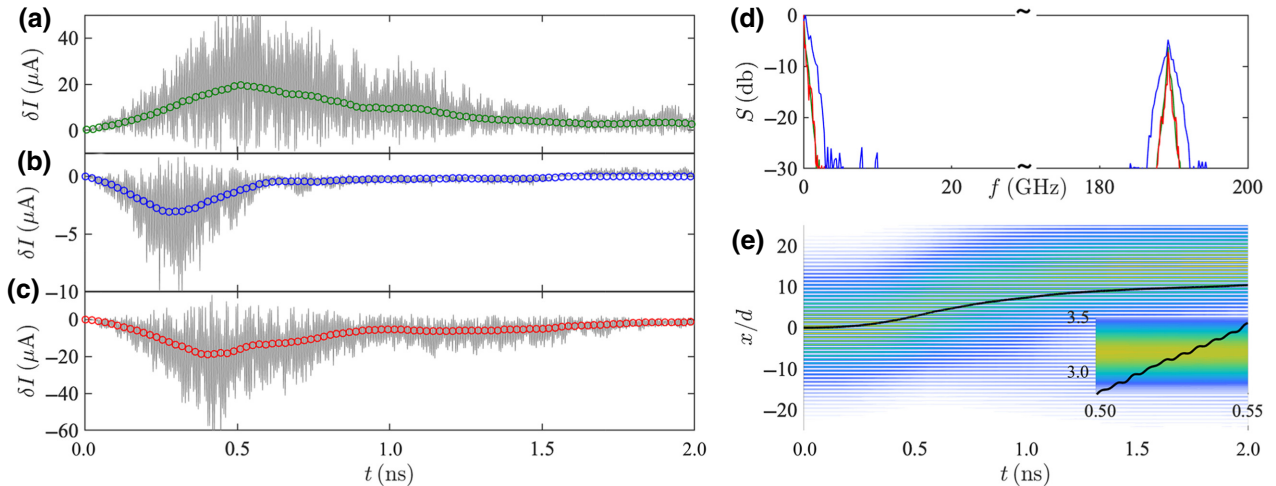


FIG. 2. (a)–(c) The time-dependent incremental current $\delta I(t)$ calculated for $V_0 =$ (a) -100 mV, (b) 0 mV, and (c) 100 mV, taking $\epsilon_a = 1.5 \times 10^{-4}$. The gray curves show the signal and the colored curves are calculated using the moving-average method with a 12.5-GHz cutoff frequency. (d) The Fourier spectra S of the (gray) signals in (a)–(c). The colors of the Fourier spectra correspond to those of the respective averaged signals in (a), (b), and (c). (e) Color maps: the evolution of the probability density (yellow = high) of the acoustically driven electron wave packet calculated for $V_0 = -100$ mV, as in (a), shown enlarged in the lower right inset. The black curves show the averaged electron trajectory $\langle x \rangle(t)$, revealing the drift and superimposed oscillations (inset) also seen in the wave-packet dynamics.

by the factor

$$\beta = (\epsilon_a D \Delta_{\text{SL}} / \pi)^{1/2} (d / \hbar v_s), \quad (4)$$

where Δ_{SL} is the width of the SL miniband and $D \approx 10$ eV is the deformation potential for GaAs [34,35]. Within a semiclassical picture, these fast oscillations can be associated with pendulumlike motion of electrons in the propagating acoustic (strain) potential [7]. Physically, the frequency up-conversion results from the electron orbits being pushed through the SL by the acoustic pulse train and perturbed by the passage of successive maxima and minima in the pulse. To a good approximation, the resulting orbital motion comprises drift modulated by a sinusoidal oscillation at the up-converted frequency, which is determined within a semiclassical model in Ref. [6], where Eq. (4) is derived. This electron motion is equivalent to that of a driven pendulum oscillating at the up-converted frequency [7]. The validity of the semiclassical analyses in Refs. [6,7] is confirmed by our full quantum-mechanical analysis, which reveals, first, that the mean position of the electron wave packet closely follows the semiclassical orbit and, second, that the semiclassical up-conversion frequency predicted by Eq. (4) is in good quantitative agreement with that found from the full quantum dynamics. The effect of the strain pulse also has some similarities with the effects of nonlinear acoustic waves in pure gallium [36]. For our experimental SL, we estimate $\Delta_{\text{SL}} \approx 3.4$ meV, which yields $\beta = 3.79$. This value agrees well with the 4.1 up-conversion factor demonstrated in Fig. 2(d).

This theoretical analysis is supported by our experiments. A comparison of the time-dependent incremental current $\delta I(t)$ calculated numerically using Eqs. (1)–(3) and measured experimentally for $\epsilon_a = 1.5 \times 10^{-4}$ is presented in Fig. 3. The green, blue, and red empty circles (simulations) and solid curves (measurements) correspond to

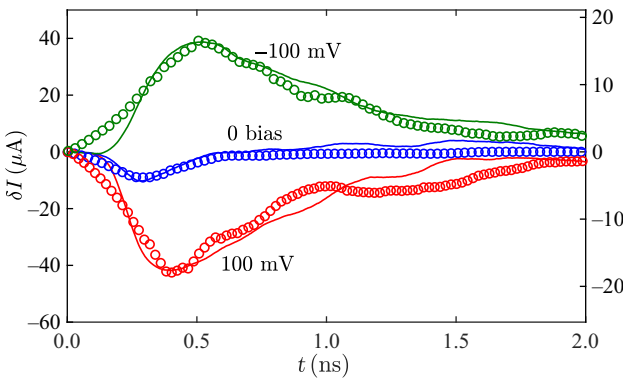


FIG. 3. Typical current pulses $\delta I(t)$ calculated numerically (open circles, right axis) and experimentally measured (solid curves, left axis) for $V_0 = +100$ mV (red), -100 mV (green), and 0 (blue), $\epsilon_a = 1.5 \times 10^{-4}$.

$V_0 = -100$ mV, 0 mV, and 100 mV, respectively. Since the measurements of $\delta I(t)$ are made using an oscilloscope with a 12.5-GHz bandwidth, we apply to our calculated $\delta I(t)$ signals a moving average filter with a cutoff frequency equal to the bandwidth of the oscilloscope [see also the empty circles in Figs. 2(a)–2(c)]. The calculated $\delta I(t)$ (empty circles, right axis) characteristics exhibit clear qualitative agreement with both the shape and polarity of the experimentally measured $\delta I(t)$ curves (solid line, left axis). Interestingly, the polarity of the response current is opposite to that of the bias. The start of the leading edge of $\delta I(t)$ corresponds to the arrival of the strain pulse at the contact. The subsequent decay of $\delta I(t)$ is determined by the duration of the strain pulses [21] [see the inset of Fig. 1(b)] and their reflections from the boundaries of the SL. The blue curves show that a nonzero $\delta I(t)$ response is generated even when $V_0 = 0$, demonstrating the direct effect of the strain pulses on charge transport in the SL, which is amplified further when $V_0 \pm 100$ mV. The scaling factor between the simulated (right axis) and measured (left axis) current pulses may originate from simplifications made in our model; in particular, the omission of the complex high-frequency charge dynamics in the contact regions [27,37] and the parasitic frequency-dependent reactance of the contacts and leads [28].

Next, we study how the peak deformation stain ϵ_a and bias voltage V_0 , applied to the SL, affect the amplitude δI_a of the generated current pulses $\delta I(t)$, where δI_a is defined as the maximum (minimum) of $\delta I(t)$ in the case of positive (negative) polarity of the pulse (see Fig. 3). Figure 4 summarizes our analysis of the current response to variation of V_0 and ϵ_a , where the calculated δI_a values are shown after filtering with a bandwidth of 12.5 GHz. The empty circles in Fig. 4(a) show δI_a values calculated numerically for $\epsilon_a = 1.27 \times 10^{-4}$ and various V_0 values. The positive or negative values of δI_a reflect the polarity of the current

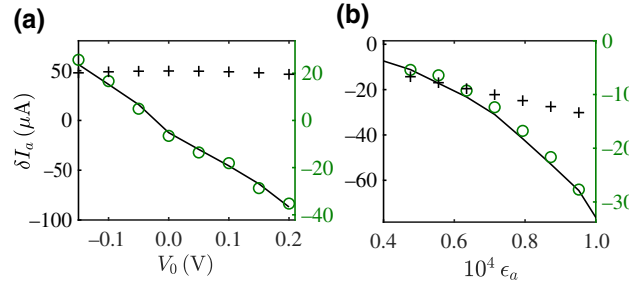


FIG. 4. The calculated (symbols, right axis) and measured (solid lines, left axis) variation of the current-pulse amplitude δI_a with applied bias V_0 (a) and strain-pulse amplitude ϵ_a in the train (b). The open circles are the numerical calculations. The crosses are the values [divided by a factor of 20 in (a), and of -20 in (b)] calculated from an analytical model developed to describe the response of the SL to irradiation by an electromagnetic wave [see the Appendix and Eq. (A2)].

pulses (see also Fig. 3). Increasing the bias magnitude $|V_0|$ leads to proportional change in δI_a . The polarity of the response current changes at $V_0 \approx 50$ mV, reflecting the fact that even in the absence of an applied bias, i.e., $V_0 = 0$, the acoustic excitation generates a current response with negative polarity (see Fig. 3). The open circles in Fig. 4(b) show the numerically calculated $\delta I_a(\epsilon_a)$ dependence for $V_0 = 300$ mV. These calculations show that the magnitude of the current pulses grows nonlinearly and monotonically as the strain stimuli become stronger and preserves the polarity of the current pulse defined by the bias V_0 .

The experimentally measured $\delta I_a(V_0)$ and $\delta I_a(\epsilon_a)$ variations are presented in Figs. 4(a) and 4(b) by solid lines. In all cases, the numerically calculated values demonstrate excellent agreement with the measured characteristics, thus confirming the validity of our numerical model.

Furthermore, we compare the response of the SL to the acoustic excitations with known results on the rectification and detection of electromagnetic waves by semiconductor tunneling devices [31,33,38], based on a theoretical framework that we discuss briefly in the Appendix. To facilitate this comparison, we calculate the amplitude of the time-dependent response of the SL to electromagnetic irradiation (photons), which produces a potential with the same frequency and amplitude as the deformation pulses (coherent phonons) in our study [see Eq. (A2) in the Appendix]. We note that since the electromagnetic waves propagate through the lattice at the speed of light and their wavelength in the gigahertz range significantly exceeds the SL length L , propagation effects and any spatial dependence of the potential are neglected in this alternative model. Plots of $\delta I_a(V_0)$ and $\delta I_a(\epsilon_a)$ calculated using analytical formula (A2) are shown by crosses in Figs. 4(a) and 4(b). These figures reveal that the values of δI_a estimated from Eq. (A2) significantly deviate both from the experimental and numerical results; compare the positions of the circles, solid line, and crosses in the figure. This divergence is not only quantitative, with a scaling factor of at least ± 20 , but also qualitative, since the dependence of the theoretical and experimental curves on V_0 and ϵ_a differs significantly. This difference highlights that quantum tunneling due to strain waves can only be understood if the propagation of the wave through the material is explicitly included.

Finally, we show that strain-pulse propagation could potentially induce even higher frequency up-conversion, reaching the terahertz regime. In particular, in the nearly-free-electron regime, i.e., when the barrier width, b , is much smaller than the SL period, d , the miniband width, Δ_{SL} , approaches $\hbar^2\pi^2/(2md^2)$ [39]. In this regime, d can be chosen to maximize the value of β given in Eq. (4). An up-conversion factor $\beta = 19.02$ close to the theoretical maximum can be achieved by taking $d = 9.8$ nm with a monolayer thick AlAs barrier the thickness of which equals the GaAs lattice constant, $b = 0.565$ nm. Figure 5(a) shows Fourier spectra of the $\delta I(t)$ current pulses

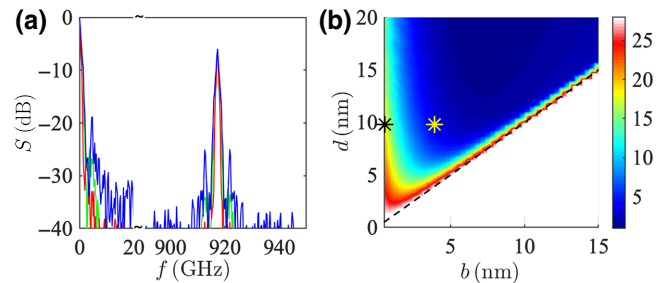


FIG. 5. (a) The Fourier spectra, S , of the $\delta I(t)$ oscillations calculated for the SL with a monolayer barrier when $V_0 = +100$ mV (red), -100 mV (green), and 0 (blue), taking $\epsilon_a = 1.5 \times 10^{-4}$. (b) The color map of the frequency up-conversion factor, β , calculated as a function of the SL barrier width, b , and period, d . The value of β is independent from V_0 . The black asterisk corresponds to the SL parameters in (a) and the yellow asterisk to those of the original SL considered earlier in the paper.

calculated for the same acoustic strain signal considered above ($\epsilon_a = 1.5 \times 10^{-4}$), taking $V_0 = 100$ mV (red curve), 0 mV (blue curve), and -100 mV (green curve). For all V_0 values, the peaks in the Fourier spectra occur at a frequency $f = 917$ GHz, which is approximately 19.9 times larger than the 46-GHz frequency of the acoustic oscillations and is consistent with the up-conversion factor $\beta = 19.02$ predicted from Eq. (4). To further investigate how the SL parameters affect frequency up-conversion, the color map in Fig. 5(b) shows the value of β calculated from Eq. (4) as a function of b and d . The parameters of the original SL considered above ($b = 3.9$ nm, $d = 9.8$ nm), for which $\beta = 3.74$, are marked by the yellow asterisk, while those for the SL with a monolayer barrier ($b = 0.565$ nm, $d = 9.8$ nm) with $\beta = 19.02$ are shown by the black asterisk. Of particular note is the bottom left region of the attainable (b, d) space (i.e., above the dashed line), where very small b values give $\beta = 29$, corresponding to an up-converted current oscillation frequency of 1.33 THz.

IV. CONCLUSION AND OUTLOOK

In conclusion, we investigate the dc and time-dependent response of a weakly coupled SL to a hypersonic strain pulse train. In theory and experiment, we show that increasing either the applied bias voltage or the amplitude of the acoustic stimuli changes the magnitude of the electric current pulses induced in the SL. Our quantum model, based on the time-dependent Schrödinger equation with a propagating potential generated by strain stimuli, reproduces the shape and polarity of current pulses generated in the SL for various intensities of acoustic wave packets and a range of applied bias voltage. Remarkably, the simulations predict current oscillations with a frequency much higher than that of the strain pulse train. The quantitative agreement that we report between the theoretical

and experimental behavior of the current pulses supports our prediction of these high-frequency oscillations. Our results highlight the potential of SL devices as tunable acoustoelectric transducers for generating high-frequency (subterahertz to terahertz) electromagnetic waves.

Recent experiments have shown that current oscillations in SLs can now achieve gigahertz-terahertz radiative output powers of the order of 0.1% of the electrical power supplied to the device [40]. From Fig. 4(a) of our paper, the electrical power of the frequency-up-converted current oscillations is approximately $100 \mu\text{A} \times 0.2 \text{ V} = 20 \mu\text{W}$. We therefore expect around 20 nW radiative output power for a single SL device. However, synchronization of N SLs can yield an N^2 -fold increase in the output power of the electromagnetic emission [41]. So, for the frequency-up-conversion process that we report, a 10×10 array of SLs might produce radiative emission approaching the milliwatt range.

Our quantum model is also applicable to a range of other device architectures, materials, and acoustic wave parameters and can therefore be applied widely to study high-frequency acoustoelectric effects in heterostructures including devices based on two-dimensional and van der Waals materials [42,43] and, even more generally, to cold-atom transport in periodic optical lattices driven by a propagating potential [44].

ACKNOWLEDGMENTS

The work was supported by EPSRC (Grants No. EP/M016161/1 and No. EP/M016099/1). We thank Professor J. Cunningham, Dr. N. Hunter, Professor G. Davies, and Professor E. Linfield from the University of Leeds, and Dr. S. Heywood and Mr. N. Priestley from the Teledyne-e2v Microwave Technology Centre for insightful discussions.

APPENDIX: TUNNEL CURRENT IN SUPERLATTICES UNDER PHOTON-PHONON EXCITATION

We gain further insight into our results by deriving an analytical model adapted from the theory of nonlinear single-particle tunnel junctions under electromagnetic irradiation [38]. Previously, we have demonstrated that coherent acoustic waves can be rectified in a SL via a similar process to the rectification of electromagnetic waves in such structures [21]. Here, we extend the theoretical framework used in Ref. [21] to estimate the magnitude of the electric pulses induced by a strain wave packet in the biased SL.

In a weakly coupled SL, electrons propagate through the lattice via quantum-mechanical tunneling between neighboring quantum wells. The interaction of a SL electron with a coherent strain wave, with frequency ω , will cause the electron to absorb a phonon of energy $\hbar\omega$. Therefore, assuming that tunneling between the quantum wells

is independent, i.e., affected only by the properties of adjacent wells, the tunneling rate will be affected only by the energy of the excitation, rather than its phase. This assumption neglects any effects caused by changes of the phase of the acoustic wave as it propagates along the SL. Then the acoustic wave can be described by an effective oscillating electric potential $V_{\text{ac}}(t) = (\epsilon_a D L)/(ed) \sin(\omega t)$ [21,38], where D is the deformation potential, L is the SL length, e is the electron charge, and d is the SL period.

If the conductance of the SL varies slowly on the voltage scale $\hbar\omega/e$ and $(\epsilon_a D L)/(\hbar\omega d)$ is small enough, we can estimate the dc and time-dependent current response classically by considering the detection and rectification of an effective voltage signal $V_0 + (\epsilon_a D L)/(ed \sin \omega t)$ by a device with a current-voltage characteristic $I_0(V_0)$. In this case, the amplitude of the time-dependent current component δI_a can be estimated as [21,33,38]

$$\delta I_a(V_0, \epsilon_a) = \left(\frac{\epsilon_a D L}{ed} \right) \frac{dI_0(V_0)}{dV_0}. \quad (\text{A1})$$

Remarkably, the shape of the $I_0(V_0)$ curve is accurately described by a cubic polynomial $I_0(V_0) = aV_0 - bV_0^3$, which is widely used to approximate the N-shaped current-voltage characteristics of tunnel devices [45]. A good fit to the data is obtained using the least-squares method [see the crosses in Fig. 1(b)], which gives $a = 1.65 \times 10^{-2} \text{ S}^{-1}$ and $b = 9.1 \times 10^{-3} \text{ SV}^{-2}$.

Substitution of the polynomial approximation of the current-voltage characteristics, $I_0(V_0) = aV_0 - bV_0^3$, into Eq. (A1) gives

$$\delta I_a(V_0, \epsilon_a) = \epsilon_a D L / (ed) (a - 3bV_0^2). \quad (\text{A2})$$

The corresponding dependencies of δI on V_0 and ϵ_a are shown by crosses in Fig. 4.

-
- [1] C. Thomsen, J. Strait, Z. Vardeny, H. J. Maris, J. Tauc, and J. J. Hauser, Coherent Phonon Generation and Detection by Picosecond Light Pulses, *Phys. Rev. Lett.* **53**, 989 (1984).
 - [2] G. L. Eesley, B. M. Clemens, and C. A. Paddock, Generation and detection of picosecond acoustic pulses in thin metal films, *Appl. Phys. Lett.* **50**, 717 (1987).
 - [3] A. V. Akimov, C. L. Poyser, and A. J. Kent, Review of microwave electro-phononics in semiconductor nanostructures, *Semicond. Sci. Technol.* **32**, 053003 (2017).
 - [4] D. R. Fowler, A. V. Akimov, A. G. Balanov, M. T. Greenaway, M. Henini, T. M. Fromhold, and A. J. Kent, Semiconductor charge transport driven by a picosecond strain pulse, *Appl. Phys. Lett.* **92**, 232104 (2008).
 - [5] M. T. Greenaway, A. G. Balanov, D. Fowler, A. J. Kent, and T. M. Fromhold, Using sound to generate ultra-high-frequency electron dynamics in superlattices, *Microelectron. J.* **40**, 725 (2009).

- [6] M. T. Greenaway, A. G. Balanov, D. Fowler, A. J. Kent, and T. M. Fromhold, Using acoustic waves to induce high-frequency current oscillations in superlattices, *Phys. Rev. B* **81**, 235313 (2010).
- [7] A. Apostolakis, M. K. Awodele, K. N. Alekseev, F. V. Kusmartsev, and A. G. Balanov, Nonlinear dynamics and band transport in a superlattice driven by a plane wave, *Phys. Rev. E* **95**, 062203 (2017).
- [8] S. L. Heywood, B. A. Glavin, R. P. Beardsley, A. V. Akimov, M. W. Carr, J. Norman, P. C. Norton, B. Prime, N. Priestley, and A. J. Kent, Heterodyne mixing of millimetre electromagnetic waves and sub-THz sound in a semiconductor device, *Sci. Rep.* **6**, 30396 (2016).
- [9] A. J. Kent, R. N. Kini, N. M. Stanton, M. Henini, B. A. Glavin, V. A. Kochelap, and T. L. Linnik, Acoustic Phonon Emission from a Weakly Coupled Superlattice under Vertical Electron Transport: Observation of Phonon Resonance, *Phys. Rev. Lett.* **96**, 215504 (2006).
- [10] P. D. Batista, M. Gustafsson, M. M. de Lima, Jr., M. Beck, V. I. Talyanskii, R. Hey, P. V. Santos, M. P. Delsing, and J. Rarity, Acousto-electric single-photon detector, *Proc. SPIE* **6583**, 658304 (2007).
- [11] V. I. Talyanskii, J. M. Shilton, M. Pepper, C. G. Smith, C. J. B. Ford, E. H. Linfield, D. A. Ritchie, and G. A. C. Jones, Single-electron transport in a one-dimensional channel by high-frequency surface acoustic waves, *Phys. Rev. B* **56**, 15180 (1997).
- [12] J. Cunningham, V. I. Talyanskii, J. M. Shilton, M. Pepper, A. Kristensen, and P. E. Lindelof, Single-electron acoustic charge transport on shallow-etched channels in a perpendicular magnetic field, *Phys. Rev. B* **62**, 1564 (2000).
- [13] K. J. Ahn, F. Milde, and A. Knorr, Phonon-Wave-Induced Resonance Fluorescence in Semiconductor Nanostructures: Accoustoluminescence in the Terahertz Range, *Phys. Rev. Lett.* **98**, 027401 (2007).
- [14] J. R. Gell, M. B. Ward, R. J. Young, R. M. Stevenson, P. Atkinson, D. Anderson, G. A. C. Jones, D. A. Ritchie, and A. J. Shields, Modulation of single quantum dot energy levels by a surface-acoustic-wave, *Appl. Phys. Lett.* **93**, 081115 (2008).
- [15] E. S. K. Young, A. V. Akimov, M. Henini, L. Eaves, and A. J. Kent, Subterahertz Acoustical Pumping of Electronic Charge in a Resonant Tunneling Device, *Phys. Rev. Lett.* **108**, 226601 (2011).
- [16] C. L. Poyser, A. V. Akimov, R. P. Campion, and A. J. Kent, Coherent phonon optics in a chip with an electrically controlled active device, *Sci. Rep.* **5**, 8279 (2015).
- [17] C. Brüggemann, A. V. Akimov, A. V. Scherbakov, M. Bombeck, C. Schneider, S. Höfling, A. Forchel, D. R. Yakovlev, and M. Bayer, Laser mode feeding by shaking quantum dots in a planar microcavity, *Nat. Photonics* **6**, 30 (2012).
- [18] D. Wigger, T. Czerniuk, D. E. Reiter, M. Bayer, and T. Kuhn, Systematic study of the influence of coherent phonon wave packets on the lasing properties of a quantum dot ensemble, *New J. Phys.* **19**, 073001 (2017).
- [19] C. J. Stanton, G. D. Sanders, R. Liu, G. W. Chern, C.-K. Sun, J. S. Yahng, Y. D. Jho, J. Y. Sohn, E. Oh, and D. S. Kim, Coherent phonons, nanoseismology and THz radiation in InGaN/GaN heterostructures, *Superlatt. Microstruct.* **34**, 525 (2003).
- [20] M. R. Armstrong, E. J. Reed, Ki.-Y. Kim, J. H. Gownia, W. M. Howard, M. William, E. L. Piner, and J. C. Roberts, Observation of terahertz radiation coherently generated by acoustic waves, *Nat. Phys.* **5**, 285 (2009).
- [21] C. L. Poyser, A. V. Akimov, A. G. Balanov, R. P. Campion, and A. J. Kent, A weakly coupled semiconductor superlattice as a harmonic hypersonic-electrical transducer, *New J. Phys.* **17**, 083064 (2015).
- [22] A. V. Scherbakov, P. J. S. van Capel, A. V. Akimov, J. I. Dijkhuis, D. R. Yakovlev, T. Berstermann, and M. Bayer, Chirping of an Optical Transition by an Ultrafast Acoustic Soliton Train in a Semiconductor Quantum Well, *Phys. Rev. Lett.* **99**, 057402 (2007).
- [23] F. Bloch, About the quantum mechanics of electrons in crystal lattices, *J. Phys.* **52**, 555 (1929).
- [24] L. Esaki and R. Tsu, Superlattice and negative differential conductivity in semiconductors, *IBM J. Res. Dev.* **14**, 61 (1970).
- [25] T. M. Fromhold, A. Patanè, S. Bujkiewicz, P. B. Wilkinson, D. Fowler, D. Sherwood, S. P. Stapleton, A. A. Krokhin, L. Eaves, M. Henini, N. S. Sankeshwar, and F. W. Sheard, Chaotic electron diffusion through stochastic webs enhances current flow in superlattices, *Nature* **428**, 726 (2004).
- [26] M. T. Greenaway, A. G. Balanov, E. Schöll, and T. M. Fromhold, Controlling and enhancing terahertz collective electron dynamics in superlattices by chaos-assisted miniband transport, *Phys. Rev. B* **80**, 205318 (2009).
- [27] A. G. Balanov, M. T. Greenaway, A. A. Koronovskii, O. I. Moskalenko, A. O. Selskii, T. M. Fromhold, and A. E. Kramov, The effect of temperature on the nonlinear dynamics of charge in a semiconductor superlattice in the presence of a magnetic field, *J. Exp. Theor. Phys.* **114**, 836 (2012).
- [28] N. Alexeeva, M. T. Greenaway, A. G. Balanov, O. Makarovskiy, A. Patanè, M. B. Gaifullin, F. Kusmartsev, and T. M. Fromhold, Controlling High-Frequency Collective Electron Dynamics via Single-Particle Complexity, *Phys. Rev. Lett.* **109**, 024102 (2012).
- [29] Recent claims that stochastic webs play no part in chaos-assisted electron transport in SLs [46,47] are unfounded because they are inconsistent with the literature on stochastic web formation in the undamped driven harmonic oscillator, they neglect Lyapunov instability in the presence of electron scattering, and they fail to consider space-charge build-up, which shapes the measured current-voltage characteristics of SL devices under operating conditions and makes the electric field highly nonuniform [25–28].
- [30] K. F. Renk, E. Schomburg, A. A. Ignatov, J. Grenzer, S. Winnerl, and K. Hofbeck, Bloch oscillations and nonlinear transport in semiconductor superlattice, *Physica B: Condens. Matter* **244**, 00487 (1998).
- [31] A. Wacker, Semiconductor superlattices: A model system for nonlinear transport, *Phys. Rep.* **357**, 1 (2002).
- [32] J. Kastrup, H. T. Grahn, K. Ploog, and R. Merlin, Oscillating electric field domains in superlattices, *Solid State Electron.* **40**, 157 (1996).

- [33] A. Wacker, S. J. Allen, J. S. Scott, M. C. Wanke, and A.-P. Jauho, Possible THz gain in superlattices at a stable operation point, *Phys. Status Solidi (b)* **204**, 95 (1997).
- [34] S. Adachi, *Physical Properties of III-V Semiconductor Compounds* (Wiley, New York, 1992).
- [35] I. Gorczyca, T. Suski, E. Litwin-Staszewska, L. Dmowski, J. Krupski, and B. Etienne, Deformation potential in high electron mobility GaAs/GaAsAs heterostructures, *Jpn. J. Appl. Phys.* **32**, 135 (1993).
- [36] V. D. Fil, A. L. Gaiduk, and V. I. Denisenko, Propagation of nonlinear acoustic waves in gallium, *J. Low Temp. Phys.* **47**, 207 (1982).
- [37] V. A. Maksimenko, V. V. Makarov, A. A. Koronovskii, K. N. Alekseev, A. G. Balanov, and A. E. Hramov, The effect of collector doping on the high-frequency generation in strongly coupled semiconductor superlattice, *Europhys. Lett.* **109**, 47007 (2015).
- [38] J. R. Tucker, Quantum limited detection in tunnel junction mixers, *IEEE J. Quantum Electron.* **15**, 1234 (1979).
- [39] J. M. Chamberlain, L. Eaves, and J. C. Portal, *Electronic Properties of Multilayers and Low-Dimensional Semiconductor Structures* (Springer Science & Business Media, New York, 2012), Vol. 231.
- [40] L. Li and E. H. Linfield, High-performance GaAs/AlAs superlattice electronic devices in oscillators at frequencies 100–320 GHz, *Appl. Phys. Lett.* **112**, 172103 (2018).
- [41] M. B. Gaifullin, N. V. Alexeeva, A. E. Hramov, V. V. Makarov, V. A. Maksimenko, A. A. Koronovskii, M. T. Greenaway, T. M. Fromhold, A. Patanè, C. J. Mellor, F. V. Kusmartsev, and A. G. Balanov, Microwave Generation in Synchronized Semiconductor Superlattices, *Phys. Rev. Appl.* **7**, 044024 (2017).
- [42] E. E. Vdovin, A. Mishchenko, M. T. Greenaway, M. J. Zhu, D. Ghazaryan, A. Misra, Y. Cao, S. V. Morozov, O. Makarovskiy, T. M. Fromhold, A. Patanè, G. J. Slotman, M. I. Katsnelson, A. K. Geim, K. S. Novoselov, and L. Eaves, Phonon-Assisted Resonant Tunneling of Electrons in Graphene Boron Nitride Transistors, *Phys. Rev. Lett.* **116**, 186603 (2016).
- [43] J. D. G. Greener, A. V. Akimov, V. E. Gusev, Z. R. Kudrynskyi, P. H. Beton, Z. D. Kovalyuk, T. Taniguchi, K. Watanabe, A. J. Kent, and A. Patanè, Coherent acoustic phonons in van der Waals nanolayers and heterostructures, *Phys. Rev. B* **98**, 075408 (2018).
- [44] M. T. Greenaway, A. G. Balanov, and T. M. Fromhold, Resonant control of cold-atom transport through two optical lattices with a constant relative speed, *Phys. Rev. A* **87**, 013411 (2013).
- [45] W. F. Chow, *Principles of Tunnel Diode Circuits* (Wiley, New York, 1964).
- [46] S. M. Soskin, I. A. Khovanov, and P. V. E. McClintock, Regular Rather than Chaotic Origin of the Resonant Transport in Superlattices, *Phys. Rev. Lett.* **114**, 166802 (2015).
- [47] S. M. Soskin, I. A. Khovanov, and P. V. E. McClintock, Mechanism of resonant enhancement of electron drift in nanometer semiconductor superlattices subjected to electric and inclined magnetic fields, *Phys. Rev. B* **100**, 235203 (2019).